Published in final edited form as:
Geochim Cosmochim Acta. 2012 August 15; 91: 254–270. doi:10.1016/j.gca.2012.05.012.

Use of Microfocused X-ray Techniques to Investigate the Mobilization of As by Oxalic Acid

Karen Wovkulich[1,2,*], **Brian J. Mailloux**[3], **Benjamin C. Bostick**[2], **Hailiang Dong**[4], **Michael E. Bishop**[4], and **Steven N. Chillrud**[2]

[1]Department of Earth and Environmental Sciences, Columbia University, New York, NY, 10027, USA

[2]Lamont-Doherty Earth Observatory, Palisades, NY 10964, USA

[3]Department of Environmental Sciences, Barnard College, New York, NY 10027, USA

[4]Department of Geology, Miami University, Oxford, OH, 45056, USA

Abstract

Improved linkages between aqueous phase transport and solid-phase reactions are needed to better predict and model transport of contaminants through the subsurface. Here we develop and apply a new method for measuring As mobilization *in situ* within soil columns that utilizes synchrotron-based X-ray fluorescence. By performing these measurements *in situ* during column transport experiments, we simultaneously monitor grain-scale solid phase reactions and column-scale transport. Arsenic may be effectively mobilized by oxalic acid but the geochemical and mineralogical factors that influence the rate and extent of mobilization are not well understood. Column experiments (~4 cm long × 0.635 cm ID) using As contaminated sediments from the Vineland Chemical Company Superfund site were performed on the laboratory bench as well as in the synchrotron beamline. Microfocused synchrotron X-ray fluorescence (μSXRF) maps for As and Fe were collected at the same location in the columns (<1 mm^2) before and during treatment with 10 mM oxalic acid. The fraction of As and Fe removed by oxalic acid treatment was calculated from the change in flux-normalized counts for each pixel in the map images, and these data were used to calculate kinetic parameters over the studied area. Between 79% and 83% of the As was removed from the sediments by the oxalic acid treatment based on μSXRF data; these removal percentages agreed well with laboratory data based on column effluent (88–95%). Considerably less Fe was removed by oxalic acid treatment, 14–25% based on μSXRF counts, which is somewhat higher than the 7–9% calculated from laboratory column effluent concentrations. Microfocused X-ray absorption near edge spectroscopy (μXANES) on a subset of points indicates most of the Fe was oxidized and present as a mixture of goethite, hematite, and ferrihydrite on sand grain coatings. Treatment with oxalic acid led to subtle shifts in Fe (III) species following oxalic acid treatment, either removing ferrihydrite or transforming it to more stable oxides; however, Fe redox states were not impacted. Kinetics information extracted from μSXRF data compared favorably with rates of As removal from observed As breakthrough curves. The average pseudo-first order As removal rate constant was calculated to be 0.015 min^{-1} ± 0.002 (± average standard error, N=400) based on changes in μSXRF counts over time. The spatial variation observed in the rate constant is likely a result of differences in the mineral substrate or

*Corresponding author karenw@LDEO.columbia.edu.

As retention mechanism. Geochemical models created using the calculated As removal rate constants showed agreement with As breakthrough curves for both a small column (4.25 cm × 0.635 cm ID) and a larger column (23.5 cm × 4.2 cm ID), indicating that the processes studied using the microprobe are representative and often can be predictive of larger systems. While this work was used to understand the processes that regulate As release and transport, the methods developed here could be used to study a wide variety of reaction processes, including contaminant removal due to chemical treatment, mineral precipitation due to changing redox characteristics, and solid phase transformations.

1. INTRODUCTION

Transport of chemicals and contaminants through the subsurface are controlled by interactions with the solid phase, including adsorption-desorption and mineral dissolution/precipitation (Bone et al., 2006; Johannesson and Tang, 2009; Kaste et al., 2006; O'Day et al., 2004; Polizzotto et al., 2006). Hydrogeologic investigations attempt to parameterize these processes to describe reactive transport, however, the reactions are rarely examined directly within the solid-phase. In most traditional transport experiments at the column or field scale, measurements of aqueous compositions are made over time and these are used to infer reactions in the solid phase with little or no direct measurement of the solid phase materials (Kuhlmeier, 1997; Roden et al., 2000; Wovkulich et al., 2010). Even when solids are analyzed, the characterization methods used usually examine mineral phases at the micron-scale before or after experiments to infer potential reactions that could occur within solutions (Arai et al., 2006; Singer et al., 2009). In both cases, the different scales and phases of these measurements can complicate attempts to link the data. In this work, we develop a method in which column transport experiments are conducted within a microfocused X-ray beam to simultaneously monitor grain-scale solid phase reactions and column scale transport in order to better understand element release and transport processes. This method provides a valuable tool to link time-series measurements on the solid and liquid phases while reactions are taking place.

X-ray microprobe analysis can be a powerful tool for investigating the spatial distribution of target elements at the micron scale as well as giving insight into the speciation of those elements. Microfocused synchrotron X-ray fluorescence (μSXRF) can provide information regarding relative element abundance, distribution, and correlations between elements with micron to sub-micron spatial resolution sufficient to investigate small-scale differences and heterogeneities within a sample. These data can be integrated with spectroscopic measurements performed using X-ray absorption near edge spectroscopy (μXANES) to determine oxidation state and speciation at the grain scale. To date, numerous X-ray microprobe studies have been used to examine distribution and speciation of many elements in diverse environmental samples, including investigating As speciation and mobility in poultry litter (Arai, et al., 2003), mapping toxic elements in nematodes (Jackson, et al., 2005), and examining Pb distribution and correlations in forest soils (Kaste, et al., 2006) as well as other applications and studies (Arai et al., 2006; Denecke et al., 2007; Freeman et al., 2006; Hettiarachchi et al., 2006; Moberly et al., 2009; Negra et al., 2005; Polizzotto et al., 2005; Ryser et al., 2006; Schroth et al., 1998; Singer et al., 2009; Tokunaga et al., 2008). While these studies have provided invaluable information concerning the distribution of elements and mineral phases in solids, few link these observations to measures of dissolved concentrations directly, nor do they examine dynamic systems undergoing mineralogical changes that would influence solid-solution partitioning. To fully relate aqueous and solid-phase composition, it is preferable to directly study both the solid and the solution, and to examine their evolution over time.

Concurrent study of solids and solutions in a single experiment is complicated by the fact that the measurements used for each can differ considerably in scale and frequency. Solid-phase measurements often must be performed at the grain-scale to yield mechanistic information while aqueous concentrations are not simple to analyze at the same scale. Additionally, it may only be feasible to characterize the solid phase before and after a particular treatment, providing information on the end points of the reaction but not the progress of geochemical reactions over time. This is especially problematic for column studies, since columns generally need to be sacrificed for solid phase characterization, thereby ending the experiment (Gu et al., 2005). Even when the endpoints are evaluated, it may be difficult to quantify changes due to the heterogeneous nature of environmental samples. We extend the use of microfocused synchrotron methods to study column solids *in situ* during reaction to directly observe the evolution of elemental composition, mineralogy, and speciation over time. As part of this work, we compare reaction parameters derived at various measurement scales (microprobe solid-phase measurements and cm-scale column experiments examining effluent composition) to determine if micron-scale kinetic measurements are representative of the column-scale.

Other researchers have studied column materials using microfocused X-ray techniques, but those studies have seldom performed analyses *in situ* or during reactions. Notably, μXANES has been used to study slow changes in U, Fe, and Mn speciation over a long time period (>1 yr) as a result of organic carbon input; this study quantified mineralogical changes along the column but couldn't guarantee that the exact same spots were evaluated each time (Tokunaga et al., 2008). As a result, it was not possible to directly measure the transformation of specific phases with the data collected, nor could they quantify the rates of those transformations or link mineralogical transformations to transport properties of relevant aqueous species. We instead make repeated microfocused synchrotron X-ray measurements during chemical treatment while maintaining sample configuration; by doing so, we evaluate changes in distribution and correlation of elements due to treatment in the same sample location over time. The strength in this approach is that it quantifies relatively small changes in fluorescence intensity at the same location during the experiment. Since fluorescence intensity is proportional to concentration, these changes can be used to determine concentration changes in the solid-phase substrates over time, and thus insight into their rates of reaction. Changes in element abundance and speciation as well as correlation between elements can be evaluated on a pixel-by-pixel basis; each pixel is essentially its own kinetics experiment allowing hundreds or thousands of such experiments to take place simultaneously. The fine scale resolution of microfocused synchrotron methods also separates mineral phases into their component parts, in principle, allowing us to link variation in kinetic parameters to their underlying mineralogy. Such an approach may be useful for studying a wide variety of reaction processes in natural sediments, including contaminant removal due to chemical treatment, mineral precipitation due to changing redox characteristics, solid phase transformations, etc. In the application described here, we focus on As transport.

Arsenic is a prevalent contaminant found in drinking water supplies and at US Superfund sites (Cullen and Reimer, 1989; EPA, 2002; Mandal and Suzuki, 2002; Smedley and Kinniburgh, 2002). The mobility of As is highly dependent on its interactions with oxide bearing minerals making it critical to understand mineral scale processes in order to predict field scale transport (Dixit and Hering, 2003), and make informed decisions about managing this contaminant. Numerous studies examining As fate and transport in sediment-water mixtures have focused on adsorption and surface properties (Arai et al., 2006; Moberly et al., 2009), microcosms (Keimowitz et al., 2005; Radloff et al., 2007; van Geen et al., 2004), columns (Kocar et al., 2006; Kuhlmeier, 1997; Masue-Slowey et al., 2010), or field scale observations (van Geen et al., 2003) but few have examined the linkages between the scales.

In this study, microfocused synchrotron X-ray fluorescence (μSXRF) spectroscopy was used to monitor the removal of Fe and As from sediments in column experiments during oxalic acid treatment. Laboratory work has suggested that oxalic acid, a naturally occurring soil acid, may be added to sediments as a useful part of field remediation schemes for As where pump and treat remediation is used for groundwater treatment (Wovkulich et al., 2010), though more information is needed to understand the processes and fully evaluate the utility of oxalic acid additions to an As remediation scheme. Using μSXRF and μXANES, we investigate changes in As and Fe distribution in As contaminated sands during oxalic acid treatment as well as the rate of As removal. The goals of the work presented here are threefold: (1) to show that it is possible to run sediment column experiments in the synchrotron beamline and gather information about a particular part of the column at multiple time points during the experiment thus integrating microfocused techniques with column transport studies, (2) to use such techniques to investigate As release by oxalic acid, and (3) to use μSXRF data collected at the grain scale to calculate As release rates and determine if this rate information can be used to make predictions in larger scale systems.

2. METHODS

2.1 Field methods

Aquifer solids were obtained from a pit freshly dug down below the water table with a backhoe in the most contaminated region of the Vineland Chemical Company Superfund site, a former As-based biocide manufacturing plant. The field site has been described in detail elsewhere (Wovkulich et al., 2010). The sandy aquifer sediments used in these experiments were collected and then stored sealed in new metal paint cans at 4°C until use. Groundwater used in the column experiments was collected from a pump and treat well on site with historically low As and low Fe concentrations (7 μg/L and 230 μg/L, respectively). The unfiltered groundwater was equilibrated with the atmosphere for several days, thereby further lowering As and Fe concentrations via precipitation, before moving it to cold storage (4°C) prior to use to minimize subsequent microbial activity. The aquifer on site ranges from oxic to suboxic to anoxic. The experiments described here were carried out under oxic conditions; under anoxic conditions we might expect to see greater As mobilization, therefore, these experiments would represent a lower bound for As mobilization.

2.2 Column experiments

Four small column experiments were performed (~4 cm × 0.635 cm ID). Three columns were run in the beamline; two of the three (#87-2 and #90) were analyzed by microfocused synchrotron X-ray fluorescence (μSXRF) and two of the three (#87-1 and #87-2) were evaluated before and after transport experiments with X-ray absorption near edge spectroscopy (μXANES). Configuration of each column was maintained for repeated measurements to ensure that the analysis window was identical. The fourth small column was run in the laboratory (#73) and not in the beamline to allow for frequent effluent measurements. Each of the column experiments was performed in a similar way with only minor alterations in column length and sediment packing efficiency.

For each column, the sandy aquifer material was wet packed into a section of clear polycarbonate tube with 0.635 cm ID (McMaster-Carr). Column lengths packed with sediments were between 4.0 and 4.6 cm (#73=4.25 cm, #87-1=4.6 cm, #87-2=4.3 cm, #90=4.0 cm). The small column size was chosen based on data from larger column studies (Wovkulich et al., 2010); by using the small columns we hoped to maximize the amount of As mobilization data collected in a short amount of time (i.e., less time per pore volume) such that these studies could feasibly be performed and repeated within the synchroton beamline during the allotted beamline time. A small amount of glass wool was packed into

each end to help distribute solution over the full cross sectional area of the column; the columns were sealed with nylon end caps. The columns were oriented vertically and solutions flowed upward through the columns at a groundwater velocity of ~3.4 m/d using a peristaltic pump (Rainin Instrument Co.). The flow velocity was comparable to the estimated average groundwater flow at the study site during active pumping for treatment (2–3 m/d estimated based on site dimensions and pump rates using optimal pump and treat parameters). For columns experiments performed in the beamline, the polycarbonate walls were too thick for efficient penetration of fluorescence X-rays to the solids within the column. To address this, spectroscopy was performed through a Kapton window in the column. A section of the polycarbonate material was thinned, then covered with a layer of Kapton tape and/or X-ray transparent epoxy to prevent potential leakage.

Columns were initially treated with unamended groundwater to establish baseline conditions and allow collection of μSXRF and μXANES data within the region of interest in the beamline columns (#87-1, #87-2, #90) and to flush fine solids for the lab bench column (#73), ~1 pore volume for the lab bench column. Solutions of 10 mM oxalic acid in groundwater were then pumped through the columns for several pore volumes (approximately 17 pore volumes for #73, 39 for #87-1, 31 for #87-2, and 15 for #90). This concentration of oxalic acid is greater than those typically found in natural systems; concentrations up to 1 mM have been reported in natural soil solutions (Fox and Comerford, 1990). However, previous laboratory experiments suggest this concentration may be useful for As mobilization as part of an As remediation scheme (Wovkulich et al., 2010). The pH of the oxalic acid solution was not adjusted prior to use. Each pore volume took approximately 17–20 minutes depending on the column length. For the experiment performed on the lab bench (#73), the oxalic acid treatment was followed by 4 pore volumes of groundwater. A fraction collector (LKB Bromma) was used to collect effluent samples for the lab bench experiment (#73), approximately one sample per pore volume. No effluent subsampling was performed on the columns carried out in the synchrotron beamline; however, effluent subsampling should be possible in future beamline experiments. For the lab bench experiment, samples were prepared for trace metal analysis directly following the experiment. Because of the small volume of sample in each pore volume, effluent samples were not filtered. We do not believe this biased our results since curves of effluent Fe concentration over time were smooth (suspended colloids would produce concentration spikes) and were consistent with results from larger columns where samples were filtered through 0.45 μm filters. Effective porosity of the columns was estimated to be 0.27, based on wet packed column weight and volumetric water content as determined from previous work on similar sediments (Wovkulich et al., 2010); this porosity is also within the range determined for larger columns based on bromide tracer breakthrough curves.

2.3 Sediment digests

Samples of contaminated aquifer solids before and after column experiments with oxalic acid treatment were digested using concentrated nitric, perchloric, and hydrofluoric acids and analyzed for total As, Fe, Al, and Mn concentration (Fleisher and Anderson, 1991). Total As concentrations were corrected for recovery of a standard reference material (18% difference between certified and calculated digest values for the reference material).

2.4 Inductively coupled plasma mass spectrometry

Effluent samples and sediment digests were analyzed for As, Fe, Mn, and Al content using inductively coupled plasma mass spectrometry (ICP MS) with a high-resolution Axiom Single Collector instrument (Thermo Elemental). ^{115}In was added to each sample as an internal response standard and was used for drift correction. ^{27}Al, ^{55}Mn, ^{57}Fe, ^{75}As, and ^{115}In were analyzed with the instrument set at >8500 resolving power, which is

sufficient to resolve the ^{75}As peak from $Ar\text{-}Cl^+$ interference. Each sample and standard was run three times and averaged. Three to four point calibration curves were run at least once every 30 samples; calibration curves used for analysis of the data presented here had R^2 >0.98.

2.5 Synchrotron analyses

Microfocused X-ray fluorescence (μSXRF) and X-ray absorption studies were conducted on beam X26A at the Brookhaven National Laboratory, National Synchrotron Light Source. μSXRF scans and maps were collected in focused monochromatic mode with a Si(111) monochromator using 13 keV incident X-rays. Elemental intensities of As and Fe were recorded using a Canberra 9-element Ge Array detector with integrated count times of 2 seconds per pixel. The fluorescence spectra at each pixel were normalized to incident photon intensity, I_0. The normalized fluorescence intensity is proportional to the amount of a given element in the pixel; within a constant volume, this fluorescence intensity is also proportional to a concentration. Though true detection limits will depend upon instrument configuration and samples being studied and are more appropriately reported as atoms per area, estimated detection limits for these types of studies are functionally ~1 ppm for As and even less for Fe. μSXRF scans covered an area of 0.168 × 0.168 mm with step size of 8 μm (400 pixels for column #90) or 0.3 × 0.3 mm with step size of 10 μm (930 pixels for #87-2).

For each experiment a baseline scan was taken before oxalic acid treatment, during introduction of water. Scans were taken approximately every 20 minutes during oxalic acid treatment (#90) or once before and once after treatment with oxalic acid (#87-2). The scan intervals for #90 correspond with the time required to collect the image. Although the reaction continues throughout data collection, the interval between collection at each pixel is constant, allowing a measured change in concentration to be related directly to a change in time at a given point. The columns were not moved for the duration of the experiments to ensure that each scan and pixel was reproducibly analyzed at the same location during the course of the reaction. Several points within two of the columns (#87-1 and #87-2) were chosen for microfocused X-ray absorption near edge spectroscopy (μXANES) to examine the forms of Fe present before and after oxalic acid treatment. Data were collected at the Fe K-edge over the energy range 7050 to 7220 eV. Background correction and normalization of the μXANES spectra were performed using WinXAS software (http://www.winxas.de/). Sample spectra were compared with standard spectra; linear combination fitting was performed using sixPACK software (http://ssrl.slac.stanford.edu/~swebb/sixpack.htm) to determine the percentage of various components. A variety of standards were considered for fitting, including hematite (Fe_2O_3), goethite (FeOOH), ferrihydrite (nominally $Fe(OH)_3$), siderite ($FeCO_3$), mackinawite (nominally FeS), pyrite (FeS_2), Fe(III)-illite (an Fe(III) phyllosilicate), biotite (an Fe(II) phyllosilicate), and other silicates. Of these, fits consistently only required ferrihydrite, goethite, hematite and illite. For accurate fitting, it was essential to fit with reference spectra that were collected in transmission mode and at the same instrument resolution as this instrument. Fit errors were estimated using SixPack based on statistical parameters and reference spectrum quality and orthogonality.

2.6 PHREEQCI

One-dimensional transport and kinetic simulations were performed using PHREEQCI Version 2 (Charlton and Parkhurst, 2002). Using As removal rate constants derived from the μSXRF data and column parameters from laboratory experiments, PHREEQC models were constructed to predict the effluent As concentrations over time for column experiments of different lengths.

3. RESULTS

3.1 Sediment characterization

Sediments used for the small laboratory column experiment #73 had a total of 86 ± 1 mg/kg for As, 540 ± 79 mg/kg for Fe, and 750 ± 16 mg/kg for Al (N=2). Sediments used for synchrotron column experiments (#87-1, #87-2, #90) had a total of 80 ± 4 mg/kg for As, 555 ± 15 mg/kg for Fe, and 788 ± 71 mg/kg for Al (N=3).

3.2 Arsenic and Fe removal from columns

Microfocused synchrotron X-ray fluorescence (μSXRF) data from scans taken before and during 10 mM oxalic acid treatment of column #90 indicate significant removal of As from the sediment column due to oxalic acid treatment (Figure 1). Each map image has been matched with the closest corresponding effluent data point in terms of pore volumes for a column performed outside of the radiation hutch, column #73 (Figure 1). Arsenic released from column #73 in a large peak after introduction of 10 mM oxalic acid in the influent solution; maximum effluent As concentration was 92 mg/L. Arsenic counts for each map pixel were evaluated before and after oxalic acid treatment for the column experiments performed in the beamline (#90 and #87-2) and the percent removal at each pixel was averaged, which suggests that 79 ± 9% (± 1σ) and 83 ± 8% of the As was removed from each column, respectively (Table 1).

Arsenic distribution in the scan area in column #90 varied spatially, with the lower portion of the analysis area (pixels 1–250) generally having higher starting As counts (average ~40% higher) than the upper portion of the image (pixels 251–400) (Figure 1). The upper portion of the image tended to have slightly higher average percent As removed (82% vs. 77%), though the difference is not statistically significant. Small increases in normalized As counts were observed at specific map points early in the reaction process; these increases may be due to spectral noise or may reflect precipitation or retardation within the column. However, by the end of the experiment all points showed a significant decrease in As counts. Based on complete digest data on sediments from before and after oxalic acid treatment, percent As removal was 88% for #90 and 88% for #87-2, very similar to the 79± 9% and 83± 8% predicted by comparison of μSXRF counts. Following the oxalic acid treatment, between 80% and 95% of the As had been removed from the aquifer solids of lab bench column #73; approximately 80% As removal was calculated based on digest of materials before and after treatment of column #73 whereas the 95% value is based on effluent concentrations and volume collected compared with the starting solids concentration according to sediment digest.

The μSXRF data from scans taken before and during 10 mM oxalic acid treatment suggest considerably less Fe removal from the sediments than As (Figure 1). Based on complete digestions performed on sediments from before and after oxalic acid treatment, percent Fe removal was 12% for column #90 whereas μSXRF data predicted an average of 25% removal. Evaluating the raw normalized Fe counts for each map pixel before and after oxalic acid treatment for the column experiments performed in the beamline (#90 and #87-2) and averaging the percent removal at each pixel suggests removal of 25± 32% (column #90) and 14± 14% (column #87-2) of the Fe; however, the values of individual pixels are often negative indicating precipitation or re-adsorption rather than removal (Table 2). Fe distribution in the scan area in column #90 varied spatially, with the lower portion of the analysis area (pixels 1–250) generally having higher starting Fe counts (~35% higher, 12833 ± 9403 vs. 8359 ± 5391 counts) than the upper portion of the image (pixels 251–400) (Figure 1). Points 251–400 also tended to have somewhat higher average percent Fe removed (30% vs. 22%), though there was a large spread in the data (standard deviation was

on the order of the average). Bulk sediment digestions for column #87-2 actually suggest overall increases in Fe concentrations, which is not possible as Fe was eluted from the column but could be an artifact of sample heterogeneity since different sediment sub-samples were used to characterize initial and final Fe concentrations. The μSXRF measurements in this experiment were taken in the exact same location before and during oxalic acid treatment, which can alleviate the difficulties in making comparative measurements on different sub-samples and in fact represents an advantage for microscopic measurements rather than whole column estimates of loss. The mass of Fe collected in column effluent also can be used independently to determine the quantity of Fe mobilized in the experiment and provides a somewhat independent check of Fe loss, although it still depends on either initial or final Fe concentrations determined by digestion. Based on effluent data, approximately 7% of the Fe was mobilized from the aquifer materials of lab bench column #73, comparable to the 9% of the Fe mobilized from a larger column experiment (Wovkulich et al., 2010). Both are somewhat lower than the average Fe removal values predicted by μSXRF measurements, 14–25%.

Correlations between Fe and As counts at each pixel were also examined for column #90 before and after oxalic acid treatment (Figure 2). Arsenic and Fe are expected to be spatially related due to adsorption of As to Fe phases, with varying strength of adsorption or association. Depending on the system being studied, multiple types of associations can be present and changes in correlations following treatment can indicate preferential removal of one or more of these phases. Within a correlation plot, a single compositionally-homogeneous phase of uniform thickness would form a point; Fe and As concentrations would correspond to the relative content of each element within that homogeneous phase. However, in samples such as these that have variable thickness and are heterogeneous, a single phase would form a line. The line would start near the origin (where the sample is thin or diluted by other phases) and would extend to some maximum level, which corresponds to the thickest portion of the purest phase. Prior to oxalic acid treatment, the As vs. Fe correlation plot has a cone-shaped appearance (broad divergence at the high end of concentration ranges for both constituents) indicating presence of at least two types of As/Fe associations, one with a much higher As:Fe ratio than the other. Following the oxalic acid treatment, the linear correlation between Fe and As is stronger (R^2=0.82); the slope decreases, indicating that the As:Fe ratio is lower in residual phases, consistent with the preferential removal of As from the column.

3.3 μXANES

Select points in columns #87-1 and #87-2 (4 points in each) were evaluated by Fe microfocused X-ray absorption near edge spectroscopy (μXANES) both before and after oxalic acid treatment. μXANES spectra from each point were fit by linear combinations of spectra of several Fe species. Various standards were considered for fitting, including a variety of Fe (II) and Fe (III) species, Fe silicates, Fe oxides, and Fe sulfides (Figure 3a, b; Table 3). However, only goethite, ferrihydrite, hematite, and illite were required for successful fits and the fits were reproducible independent of starting values. Each sample point showed a majority of goethite (50% or greater) and variable percentages of hematite (Table 3). Samples typically contained minor amounts of ferrihydrite and even less illite. There was no significant quantity of Fe (II) species, nor sulfides, and these were not included in the final fits. Data points after oxalic acid treatment usually displayed a decrease in percentage of ferrihydrite and an increase in other species, notably hematite and goethite.

3.4 As and Fe removal rate

For column #90, μSXRF scans were taken every ~20 minutes; this is approximately equal to the time it takes for 1 pore volume to travel through the column (17 min). Arsenic counts for

each map pixel were recorded at these time points. Normalized As counts over time are shown for several representative pixels in Figure 4. Three of the four pixel plots clearly show a lag period after oxalic acid is first introduced where As counts do not change appreciably during the initial scans. This is followed by a steady decline in As counts and then another plateau at which point the reaction reaches some form of steady-state. These points were chosen to show the range in As removal rates and variability with time after oxalic acid was introduced.

To extract kinetics information from the decreases in As concentrations, it is necessary to derive a rate expression for the mobilization/dissolution of surface bound As by oxalic acid. However, the nature of this mobilization mechanism is not completely clear and could be explained by competitive adsorption/desorption or As release prompted by the dissolution of species to which it is sorbed (Shi et al., 2009; Zhang et al., 2005). μXANES data might suggest the latter, however, both of these are adequately described by a second-order reaction rate equation.

$$d/dt(As)_{aq} = -k[As_{absorbed}][\text{oxalic acid}]$$

This generalized equation applies to either mechanism since both involve the concentration of the same species and intrinsically, both depend on the surface area of adsorbing mineral phases, presumably primarily Fe- and Al-oxides. For rate calculations, oxalic acid concentrations can be assumed constant near input values (10 mM); previous column experiments (10 mM influent) indicated 99% recovery of oxalic acid (Wovkulich et al., 2010). The second order equation can therefore be simplified to a pseudo first-order kinetic expression for the generalized reaction,

$$As_{adsorbed} \rightarrow As_{dissolved}$$

with an integrated rate law of

$$Ln[As_{adsorbed}] = -k't + Ln[As_{absorbed}]_0$$

where $[As_{adsorbed}]$ is taken as normalized As counts, k' is the rate constant, and t is time.

$Ln[As_{adsorbed}]$ vs. time should yield a straight line with slope of $-k'$, with k' referring to the pseudo first-order rate constant for As desorption. The natural log (Ln) of normalized As counts (proportional to concentration) was plotted against time (data not shown) and a desorption rate constant was calculated from the linear region. The first few time points yielded fairly stable normalized As counts as did the last few time points. We interpret these stable periods as an initial lag in As removal occurring in the first few pore volumes and then the reaction finishing before the final scan, likely due to removal of nearly all of the extractable As. The length of the lag-phase was not uniform for each pixel, and only the linear range for each pixel was utilized to determine rate constants. A range of rate constants was observed that appeared to be separated spatially based on the different map (sediment) regions (Figure 5). The lower portion of the map (points 1–250; closer to the inlet) had an average As removal rate constant of 0.011 ± 0.001 min^{-1} (average ± average standard error); the upper portion of the map (further from the inlet; points 251–400) had a somewhat higher average As removal rate constant of 0.022 ± 0.004 min^{-1} (Figure 5). The bulk average removal rate constant for the entire map area was 0.015 ± 0.002 min^{-1}; the bulk average rate constant was converted from a time based rate to a pore volume based rate by accounting for

column dimensions, porosity, and flow rates and this pore volume based rate constant was used for PHREEQCI modeling.

A similar exercise was performed for μSXRF Fe data. Normalized Fe counts over time are shown for several pixels in Figure 4b. These plots indicate that while some pixels show slight decreases in Fe, others show no significant change, or even small increases. Pseudo-first order kinetics were applied and Fe removal rate constants were calculated from the slope of $Ln[Fe_{absorbed}]$ vs. time. All scans taken during the oxalic acid treatment were used in the rate constant calculations. The average Fe removal rate constant was 0.001 ± 0.0002 min^{-1} (average ± average standard error). Some pixels showed negative Fe removal rate constant (i.e., re-precipitation or re-adsorption) (Figure A2).

3.5 PHREEQCI

Using basic column parameters from laboratory columns and a pore volume based rate derived from the bulk As removal rate constant calculated above, one-dimensional transport and As release kinetics were modeled with PHREEQCI (Table 4). Expected effluent As concentrations were calculated and compared with the effluent As concentrations from the small (4.25 cm × 0.635 cm ID) laboratory column #73 (Figure 6a). The time based rate constant derived from μSXRF data was converted to a pore volume based rate constant by multiplying the time based rate constant, k' (min^{-1}), by the number of minutes per pore volume in column #90, the column for which the rate was originally calculated. Although the average rate constant used in these calculations is independent of As release mechanism, local variations in mechanism may locally impact release rates. A four-pore volume lag, during which no As was released, was introduced into the model to better represent the data; the lag is presumed to relate to equilibration with oxalic acid. The model data was also averaged such that there was one effluent data point per pore volume to match the sampling frequency of the small column run on the laboratory bench (#73). The PHREEQCI model calculates As release at each time step, recalculating for subsequent steps based on mass of As remaining in the sediments. In the PHREEQCI modeled small column, the maximum effluent As concentration occurred at 6 pore volumes with a magnitude of 116 mg/L; in the laboratory column (#73), the maximum effluent As concentration occurred 6.3 pore volumes after oxalic acid introduction with a magnitude of 92 mg/L (Figure 6a).

The same bulk average As removal rate constant derived from the μSXRF data was applied to describe As breakthrough in a larger sediment column (referred to as large column here). This column contained sediments collected at the same time and same location as materials used in the small columns; the column was approximately 23 cm long (23.5 cm × 4.2 cm ID) and was treated with 10 mM oxalic acid. Details regarding that laboratory column are reported elsewhere (Wovkulich et al., 2010). A three-pore volume lag, during which no As was released, was introduced into the model to better represent the data. The model data was averaged such that there was one effluent data point per 0.1 pore volumes to more closely match the sampling frequency of the column run in the laboratory. In the PHREEQCI modeled large column, the peak in effluent As occurred at 4.2 pore volumes with a magnitude of 88 mg/L; in the laboratory column, the peak in effluent As occurred 4.3 pore volumes after oxalic acid introduction with a magnitude of 100 mg/L (Figure 6b). In the PHREEQCI modeled column with pore-volume based rate, it took approximately 9 pore volumes to reach 80% As removal while in the laboratory column, it took 7 pore volumes after oxalic acid introduction.

4. DISCUSSION

4.1 As removal from columns

Performing column experiments within the microfocused synchrotron beamline has allowed integration of data from the solid phase with column transport information and shows that microscale processes observed within a small portion of the column are, at least in this case, predictive of the larger system. Microfocused synchrotron X-ray fluorescence (μSXRF) data on a small section of the column sediment indicate that an average of 79–83% of As is removed by 10 mM oxalic acid treatment over the course of the experiment based on the change in normalized As counts at individual pixels over time. Preliminary experiments where sediment sub-samples from columns were scanned before and after oxalic treatment had significant limitations. It was clear from those results that As counts had decreased, but changes in As/Fe correlations were not clear; results indicated overall Fe counts increased due to a local hotspot in the after treatment sample and no rate data could be obtained. Therefore, a method was developed during which a column experiment could be performed in real-time within the microfocused beam. In the experiments described here, the extent of Fe and As removal was consistent between μSXRF scans, column effluent, and column solids. This agreement indicates that relative concentrations determined from μSXRF scans in the same location of a sediment core over the course of a reaction can be related to macroscopic removal. Moreover, it suggests that As and Fe dissolution and transport observed within a very small (<1 mm^2) scan area can be representative of larger scale transport and that variation in removal rates observed at the micron-scale is representative of chemical or physical heterogeneity in the sediment.

Throughout the scan region, As and Fe counts decreased over the course of the experiment corresponding to the decrease in As and Fe concentrations on the solids. In initial scans of beamline column #90 (each scan took ~20 minutes), most pixels displayed near constant or modestly increasing As counts. This increase in As counts suggests that As was not removed, and actually may have locally increased over that short time interval. This may result from random noise in As counts or may indicate that advected As is accumulating, at least transiently due to initial redistribution processes. However, by the end of the experiment, no pixel showed increased As counts compared to the initial scan. Arsenic re-adsorption is likely limited due to competitive sorption between oxalic acid and arsenate (Shi et al., 2009) and removal of reactive Fe surfaces.

Although experiment #87-2 included more pore volumes of oxalic acid than #90 (31 vs. 15), cumulative As mobilization was similar in both columns (79–83%). Thus only ~80% of the As in these aquifer sediments appears to be mobilized by oxalic acid treatment; further treatment did not yield full As removal. However, this process results in fairly rapid release of a significant portion of the sediment As and may be well suited for extraction-based remediation strategies.

4.2 Fe removal from columns

There are several interesting components to the Fe data that provide mechanistic information about the mineralogy of adsorption, and the control of the underlying substrate on As removal. There is evidence for Fe re-precipitation based on the μSXRF data, which may contribute to the relatively low overall net Fe removal from the columns. Following the addition of oxalic acid to the columns, a significant number of data points or pixels consistently show Fe accumulation (an increase in normalized Fe counts over time) rather than Fe removal. For column #90, nearly 20% of the data points had ≤ 0% Fe removal (12% for #87-2) at the end of the treatment. The accumulation of Fe observed within these pixels appears to be real, and indicates that while Fe is mobilized within the column, it is not

effectively advected through the column and instead re-precipitates or re-adsorbs in other areas. Because re-precipitation of Fe is evident on the sub millimeter scale (scan area <1 mm^2) in the small columns, it is likely that re-precipitation or re-adsorption of Fe is also taking place throughout the small and large columns. The re-precipitation and re-adsorption of Fe may help to explain the limited extent of net Fe removal even though oxalic acid has been shown to complex and dissolve Fe species (Baumgartner et al., 1983; Blesa et al., 1987; Lee et al., 2007; Panias et al., 1996). SEM data also indicates that Fe removal was limited as Al and Fe coatings on quartz grains are still present following oxalic acid treatment (Appendix Figure A1; EDS spectra not shown).

Previous work has shown that in the large oxalic acid columns, Al, As and Fe breakthrough did not occur at the same time; Al began to release first, then As, followed by Fe (Wovkulich et al., 2010). This difference in breakthrough prompted us to question whether As release was predicated on Fe dissolution and transport since Fe transport appears to occur following As release. However, the μSXRF data provides direct evidence for Fe re-precipitation or re-adsorption and offers an alternate possibility; As and Fe release do happen concurrently, at least to some extent, but Fe re-precipitation, re-adsorption, and retardation within the column delay and/or suppress Fe appearance in the effluent solution.

4.3 μXANES and As:Fe correlations

The μXANES data and correlations between As and Fe counts as measured by μSXRF were examined before and after oxalic acid treatment to better understand changes in Fe mineralogy and its control on As transport (Figure 2). There is no evidence for significant change in Fe oxidation state from before to after the oxalic acid treatment, i.e., Fe species did not undergo reduction (Figure 3, Table 3). Ferrihydrite appears to have been removed by oxalic acid treatment at a variety of As- and Fe-rich locations whereas other Fe(III) minerals showed increases and no large increase in Fe(II) minerals was observed. Changes in Fe (III) species were subtle but real, even though differentiation between the various Fe (III) minerals can be difficult with XANES data. Greater differentiation between Fe (III) minerals may be possible through spectral averaging of several scans at each point before and after reaction. However, due to time limitations, it was necessary to weigh the value of kinetic versus mineralogical data when designing the beamline experiments. Here we opted to collect more kinetic data at the expense of mineralogical data.

Before oxalic acid treatment, the As vs. Fe plot contains scatter in a cone shaped pattern. Following oxalic acid treatment the As vs. Fe plot shows a stronger linear correlation (R^2=0.82), which could be influenced by several factors. Since the As in these solids is almost entirely As(V) based on bulk XANES data (not shown), it is unlikely that the stronger correlations are the result of one oxidation state of As being preferentially removed. Instead, the stronger correlations may result from the preferential removal of As from a specific adsorbing phase or phases, as suggested by the μXANES. Elemental correlations in the maps are consistent with this interpretation as the scatter in As:Fe correlations before treatment reflects interaction of As with one or more Fe bearing phases. Oxides of Mn and Al also provide sorption sites for As (Mandal and Suzuki, 2002; Smedley and Kinniburgh, 2002; Sullivan and Aller, 1996). If As was released from these sites, the correlation between As and Fe could have strengthened following oxalic acid treatment. The Fe μXANES spectra confirm that most of the Fe is present primarily as mixture of crystalline and amorphous Fe(III) oxides (Figure 3, Table 3). Since As can associate with all of these phases, the preferential extraction of ferrihydrite would remove more As than Fe because of its high surface area. This would lead to a lower As:Fe ratio following treatment, as was observed. Given the low overall removal of Fe, the change in Fe mineralogy could also reflect the transformation of ferrihydrite to more crystalline forms. Alternatively, structural changes in the ferrihydrite that occur during its partial dissolution may affect fitting. This

may be particularly problematic for goethite in that goethite and ferrihydrite often are spectrally similar. Additionally, at some data points, an increase in Fe was seen, indicating re-precipitation or re-adsorption of Fe within the column, potentially in more crystalline forms.

4.4 Rates of As removal and comparisons with PHREEQCI models

Net As removal modeled by PHREEQCI for small and large columns agree well with effluent data from the laboratory columns when using a pore volume based As removal rate (Figure 6). The size of the column is not important and based on these results, one would expect similar results on a per pore volume basis for 4 cm columns or field scale "columns." Contact time appears not to be important as 4 cm columns require ~20 min per pore volume whereas 23 cm columns require ~2.5 hrs per pore volume, yet columns still quickly achieved nearly equivalent As removal rates indicating rapid equilibrations of the removal reactions.

A lag time, where no significant As release is seen in the first few pore volumes, was necessary to include in the models to improve the match; we believe this is related to the buffering capacity and pH within the column. Oxalic acid is known to mobilize Al and Fe (Lee et al., 2007; Li et al., 2006). Therefore, one may hypothesize that removal of Al and Fe sorption sites leads to As release and As release is related to Fe release. Since Fe release occurs optimally at a pH of 2–3 (Lee et al., 2007; Panias et al., 1996), there is a lag initially in As release as the buffer capacity of the sediment is overcome. Once sediment pH is low enough and oxalic acid is therefore predominantly found as $HC^2O_4^-$, Fe and thus As release occurs (Figure 6b). In the large column, As release begins to increase ~2 pore volumes after the introduction of oxalic acid when the effluent pH is still 4.5–5. The buffer capacity of sediments early in the column may have been overcome within a short time frame leading to the initiation of As release whereas pH buffering in the later sediments kept the effluent pH high until additional effluent passed. The peak in As concentration occurs when the pH is ~2.5–3. This suggests that pH 2–3 is optimal for As release as well, perhaps because As release is linked to Fe release. Since pKa_1 for arsenate is 2.15, desorption of uncharged As species may also play a role.

A longer lag time in the models is necessary for the small column than the large, which may be partly explained by the differences in pore volume size and the volume in the tubing leading up to the laboratory columns. The small column (#73) has a pore volume of just ~0.4 mL whereas the large column has a pore volume closer to 100 mL. Oxalic acid introduction was marked from the time the tubing entered the oxalic influent bottle; the volume held by the tubing leading up to the bottom of the columns would be a much larger percentage of a pore volume for the small column than the large.

It is worth considering that other factors, besides As concentration (or counts), may be important to the removal rate on scales larger than microscale. Studies have investigated oxalic acid removal rates of Fe in various systems and have suggested that other parameters such as pH and oxalate concentration may need to be considered in rate equations (Lee et al., 2007; Lee et al., 2006). Future studies should be directed towards developing more quantitative reactive transport models including additional parameters, such as pH, effluent oxalate concentrations, precipitation of Fe phases, and As sorption. However, such models are beyond the scope of this work. Here we aimed to keep the models simple for three primary reasons. First, the models do not depend on any parameters that cannot be independently derived from the microprobe data, which allows description of As breakthrough with information gathered almost entirely from the μSXRF maps. Second, more complex models would require that additional model parameters be fit based on bulk properties, e.g. how system pH changes in response to mineral dissolution, buffering by

mineral components, etc. Such fits would not be well-constrained based on available data. However, future experiments could explore a series of columns in which a single set of macroscopic parameters could be examined by fitting and unified with variable As release kinetics. Finally, while pH and effluent Fe data are available for some of the columns, a complete set of data that would be needed to constrain a more complex model is not currently available. Measurement of pH in column effluent of the small columns is difficult with traditional electrodes. Additionally, Fe data indicates a small but overall positive release of Fe from the columns that does not match As release, which makes linking this information to an integrated model of As and Fe release difficult. While the models presented here are simplistic, they do demonstrate the ability to calculate As release kinetics and match that information with laboratory data.

5. CONCLUSIONS

We have shown that it is possible to run sediment column experiments in the synchrotron beamline and gather information about a particular part of the column at multiple time points during the experiment and integrate microfocused synchrotron techniques with column transport studies. The decrease in overall As and Fe counts over the treatment time showed that oxalic acid mobilized these species, with net As removal being greater than Fe removal. Arsenic and Fe release based on μSXRF counts from before and after oxalic acid treatment were consistent with laboratory column effluent data. The small scale (<1 mm^2) μSXRF maps, therefore, provide information regarding net removal and removal rates consistent with the bulk material (small column and large column).

We used a combination of μSXRF data and PHREEQCI models to investigate As release rate information. Columns modeled with a pore volume based As removal rate agreed fairly well with laboratory effluent data for both small and large columns. This would suggest one could expect similar results in the field on a per pore volume basis. However, extrapolating the rate information to larger systems may be complicated by other factors that impact large-scale transport (diffusion, dispersion, preferential transport pathways, increased variability in concentrations and matrix composition, etc.); a more complete and more effective rate equation might require information on additional parameters such as pH or oxalic acid concentration.

Performing column studies within a microfocused synchrotron beamline offers a powerful approach for studying microscale changes in element abundance and distribution over time and relating these changes to column transport. Since the same area of sediment is examined each time, reaction rate information can also be obtained for each pixel in the map area; this precisely focused approach essentially allows study of hundreds of reactions at once and provides more statistically relevant reaction rates. These microfocused synchrotron techniques should find application for studying a wide variety of reaction processes.

Acknowledgments

The authors would like to thank the US EPA, the US Army Core of Engineers, and Sevenson Environmental at the Vineland Superfund Site for access to samples and support on site. Portions of this work were conducted at beamline X26a National Synchrotron Light Source (NLSL), Brookhaven National Laboratory. X26a is supported by the U.S. Department of Energy (DOE) - Geosciences (DE-FG02-92ER14244 to The University of Chicago - CARS) and DOE - Office of Biological and Environmental Research, Environmental Remediation Sciences Div. (DE-FC09-96-SR18546 to the University of Kentucky). Use of the NSLS was supported by DOE under Contract No. DE-AC02-98CH10886. The authors would like to thank Antonio Lanzirotti for assistance with microprobe work on beamline X26a. This work was supported by the Superfund Research Program (NIEHS Grant ES010349). Additional support was provided by NIEHS Grant ES0090890. This is LDEO publication xxxx.

APPENDIX

SEM methods

Scanning electron micrograph images of solids were obtained before and after treatment with oxalic acid. Images were collected using a Zeiss Supra 35 VP FEG SEM that was operated at an accelerating voltage of 21–22 kV. The instrument was equipped with energy dispersive spectroscopy (EDS); EDS spectra of specific grains allowed qualitative evaluation of dominant elements in the grain.

SEM results

Scanning electron microscopy (SEM) was used to visualize sand grains from samples with and without oxalic acid treatment (Figure A1a before treatment, Figure A1b, sediments from column #90 after treatment). Micrographs show no gross morphological changes in the coatings on the quartz grains. Furthermore, energy dispersive spectroscopy (EDS) results show that Fe and Al coatings were present in samples both with and without oxalic acid treatment and that As was associated with these coatings (data not shown).

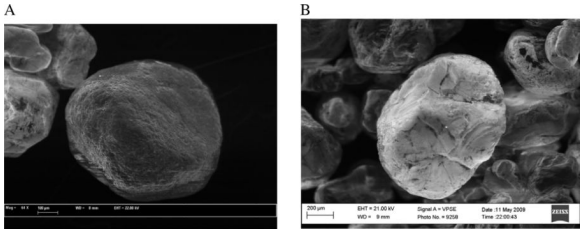

Figure A1. Scanning electron micrograph images of aquifer sediments (a) prior to treatment with oxalic acid and (b) following treatment with oxalic acid. The image in (b) shows sediments following column experiment #90, which took place at the synchrotron beamline. Both samples were also analyzed by energy dispersive spectroscopy (EDS); while Al and Fe peaks decreased in size from before to after oxalic acid treatment, the peaks were still present.

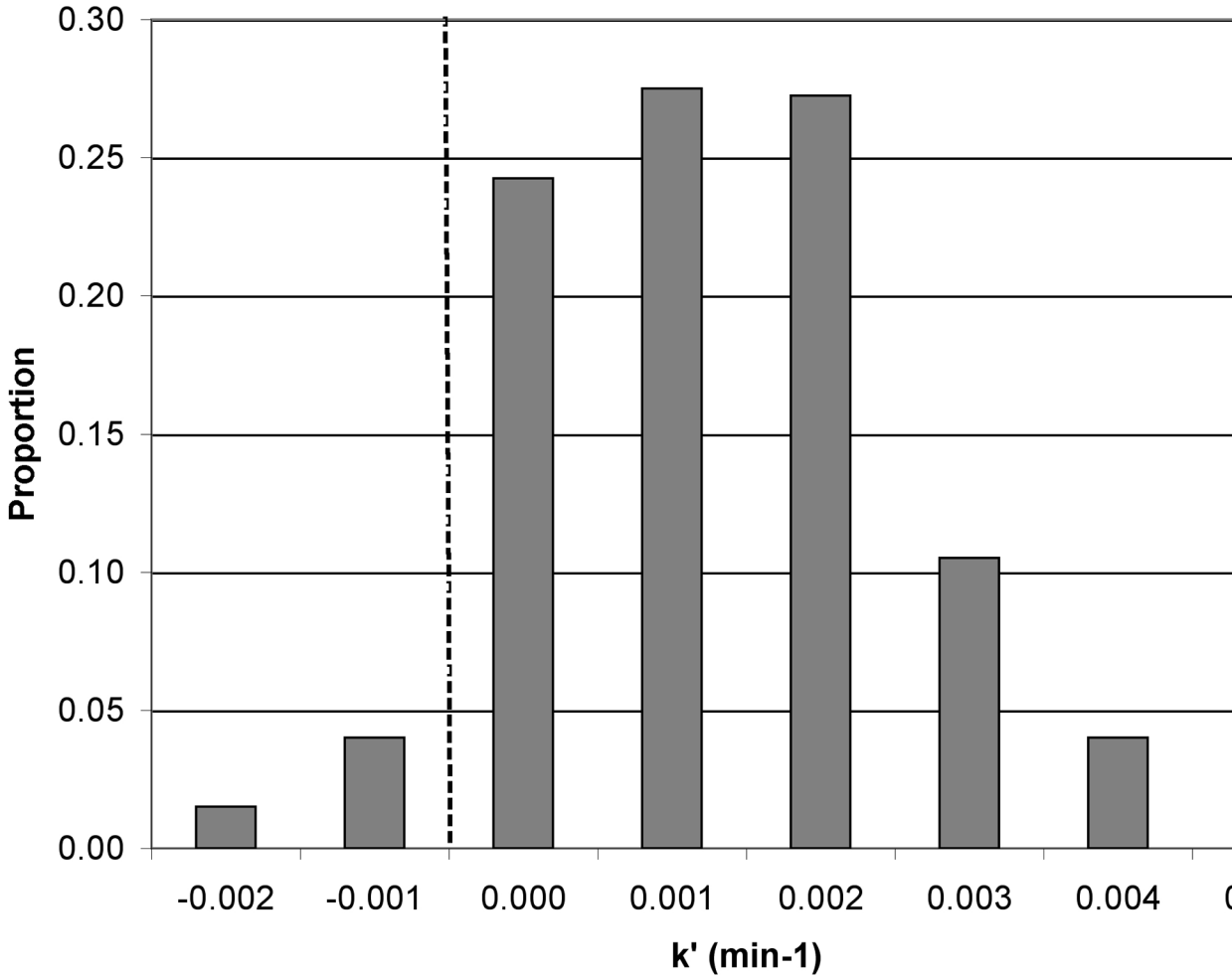

Figure A2. Distribution of rate constants of Fe removal. Histogram showing the proportion of different rate constants of Fe removal in the section of column #90 analyzed by μSXRF. The average removal rate constant is 0.001 min^{-1}.

REFERENCES

Arai Y, Lanzirotti A, Sutton SR, Newville M, Dyer J, Sparks DL. Spatial and temporal variability of arsenic solid-state speciation in historically lead arsenate contaminated soils. Environmental Science & Technology. 2006; 40(3):673–679. [PubMed: 16509302]

Baumgartner E, Blesa MA, Marinovich HA, Maroto AJG. Heterogeneous Electron-Transfer as a Pathway in the Dissolution of Magnetite in Oxalic-Acid Solutions. Inorganic Chemistry. 1983; 22(16):2224–2226.

Blesa MA, Marinovich HA, Baumgartner EC, Maroto AJG. Mechanism of Dissolution of Magnetite by Oxalic Acid-Ferrous Ion Solutions. Inorganic Chemistry. 1987; 26(22):3713–3717.

Bone SE, Gonneea ME, Charette MA. Geochemical cycling of arsenic in a coastal aquifer. Environmental Science & Technology. 2006; 40(10):3273–3278. [PubMed: 16749693]

Charlton SR, Parkhurst DL. PHREEQCI: A graphical user inerface to the geochemical model PHREEQC. USGS Survey Fact Sheet. 2002 FS-031-02.

Cullen WR, Reimer KJ. Arsenic speciation in the environment. Chemical Reviews. 1989; 89:713–764.

Denecke MA, Somogyi A, Janssens K, Simon R, Dardenne K, Noseck U. Microanalysis (micro-XRF, micro-XANES, and micro-XRD) of a tertiary sediment using microfocused synchrotron radiation. Microscopy and Microanalysis. 2007; 13(3):165–172. [PubMed: 17490498]

Dixit S, Hering JG. Comparison of arsenic(V) and arsenic(III) sorption onto iron oxide minerals: Implications for arsenic mobility. Environmental Science & Technology. 2003; 37(18):4182–4189. [PubMed: 14524451]

EPA. Arsenic treatment technologies for soil, waste, and water. 2002 http://www.clu-in.org/download/remed/542r02004/arsenic_report.pdf.

Fleisher MQ, Anderson R. Particulate matter digestion (from mg to 10's of g) and radionuclide blanks. Marine Particle Analysis and Characterization; American Geophysical Union. 1991:221–222.

Fox TR, Comerford NB. Low-molecular-weight organic-acids in selected forest soils of the southeastern USA. Soil Science Society of America Journal. 1990; 54(4):1139–1144.

Freeman JL, Zhang LH, Marcus MA, Fakra S, McGrath SP, Pilon-Smits EAH. Spatial imaging, speciation, and quantification of selenium in the hyperaccumulator plants Astragalus bisulcatus and Stanleya pinnata. Plant Physiology. 2006; 142(1):124–134. [PubMed: 16920881]

Gu BH, Wu WM, Ginder-Vogel MA, Yan H, Fields MW, Zhou J, Fendorf S, Criddle CS, Jardine PM. Bioreduction of uranium in a contaminated soil column. Environmental Science & Technology. 2005; 39(13):4841–4847. [PubMed: 16053082]

Hettiarachchi GM, Scheckel KG, Ryan JA, Sutton SR, Newville M. mu-XANES and mu-XRF investigations of metal binding mechanisms in biosolids. Journal of Environmental Quality. 2006; 35(1):342–351. [PubMed: 16397110]

Johannesson KH, Tang J. Conservative behavior of arsenic and other oxyanion-forming trace elements in an oxic groundwater flow system. Journal of Hydrology. 2009; 378:13–28.

Kaste JM, Bostick BC, Friedland AJ, Schroth AW, Siccama TG. Fate and speciation of gasoline-derived lead in organic horizons of the northeastern USA. Soil Science Society of America Journal. 2006; 70(5):1688–1698.

Keimowitz AR, Simpson HJ, Stute M, Datta S, Chillrud SN, Ross J, Tsang M. Naturally occurring arsenic: Mobilization at a landfill in Maine and implications for remediation. Applied Geochemistry. 2005; 20:1985–2002.

Kocar BD, Herbel MJ, Tufano KJ, Fendorf S. Contrasting effects of dissimilatory iron (III) and arsenic (V) reduction on arsenic retention and transport. Environmental Science & Technology. 2006; 40:6715–6721. [PubMed: 17144301]

Kuhlmeier PD. Sorption and desorption of arsenic from sandy soils: column studies. Journal of Soil Contamination. 1997; 6(1):21–36.

Lee SO, Tran T, Jung BH, Kim SJ, Kim MJ. Dissolution of iron oxide using oxalic acid. Hydrometallurgy. 2007; 87:91–99.

Lee SO, Tran T, Park YY, Kim SJ, Kim MJ. Study on the kinetics of iron oxide leaching by oxalic acid. International Journal of Mineral Processing. 2006; 80(2–4):144–152.

Li JY, Xu RK, Tiwari D, Ji GL. Mechanism of aluminum release from variable charge soils induced by low-molecular-weight organic acids: Kinetic study. Geochimica Et Cosmochimica Acta. 2006; 70(11):2755–2764.

Mandal BK, Suzuki KT. Arsenic round the world: a review. Talanta. 2002; 58:201–235. [PubMed: 18968746]

Masue-Slowey Y, Kocar BD, Bea Jofré SAs, Mayer KU, Fendorf S. Transport Implications Resulting from Internal Redistribution of Arsenic and Iron within Constructed Soil Aggregates. Environmental Science & Technology. 2010; 45(2):582–588. [PubMed: 21158450]

Moberly JG, Borch T, Sani RK, Spycher NF, Sengor SS, Ginn TR, Peyton BM. Heavy Metal-Mineral Associations in Coeur d'Alene River Sediments: A Synchrotron-Based Analysis. Water Air and Soil Pollution. 2009; 201(1–4):195–208.

Negra C, Ross DS, Lanzirotti A. Soil manganese oxides and trace metals: Competitive sorption and microfocused synchrotron X-ray fluorescence mapping. Soil Science Society of America Journal. 2005; 69(2):353–361.

O'Day PA, Vlassopoulos D, Root R, Rivera N. The influence of sulfur and iron on dissolved arsenic concentrations in the shallow subsurface under changing redox conditions. Proceedings of the National Academy of Sciences. 2004; 101(38):13703–13708.

Panias D, Taxiarchou M, Paspaliaris I, Kontopoulos A. Mechanisms of dissolution of iron oxides in aqueous oxalic acid solutions. Hydrometallurgy. 1996; 42(2):257–265.

Polizzotto ML, Harvey CF, Li G, Badruzzman B, Ali A, Newville M, Sutton S, Fendorf S. Solid-phases and desorption processes of arsenic within Bangladesh sediments. Chemical Geology. 2006; 228(1–3):97–111.

Polizzotto ML, Harvey CF, Sutton SR, Fendorf S. Processes conducive to the release and transport of arsenic into aquifers of Bangladesh. Proceedings of the National Academy of Sciences of the United States of America. 2005; 102(52):18819–18823. [PubMed: 16357194]

Radloff K, Cheng Z, Rahman M, Ahmed K, Mailloux B, Juhl A, Schlosser P, van Geen A. Mobilization of arsenic during one-year incubations of grey aquifer sands from Araihazar, Bangladesh. Environmental Science & Technology. 2007; 41(10):3639–3645. [PubMed: 17547190]

Roden EE, Urrutia MM, Mann CJ. Bacterial reductive dissolution of crystalline Fe(III) oxide in continuous-flow column reactors. Applied and Environment Microbiology. 2000; 66(3):1062–1065.

Ryser AL, Strawn DG, Marcus MA, Fakra S, Johnson-Maynard JL, Moller G. Microscopically focused synchrotron X-ray investigation of selenium speciation in soils developing on reclaimed mine lands. Environmental Science & Technology. 2006; 40(2):462–467. [PubMed: 16468390]

Schroth MH, Istok JD, Conner GT, Hyman MR, Haggerty R, O'Reilly KT. Spatial variability in in situ aerobic respiration and denitrification rates in a petroleum-contaminated aquifer. Ground Water. 1998; 36(6):924–937.

Shi R, Jia YF, Wang C, Shuhua Y. Mechanism of arsenate mobilization from goethite by aliphatic carboxylic acid. Journal of Hazardous materials. 2009; 163:1129–1133. [PubMed: 18752889]

Singer DM, Zachara JM, Brown GE. Uranium Speciation As a Function of Depth in Contaminated Hanford Sediments - A Micro-XRF, Micro-XRD, and Micro-And Bulk-XAFS Study. Environmental Science & Technology. 2009; 43(3):630–636. [PubMed: 19244994]

Smedley PL, Kinniburgh DG. A review of the source, behaviour and distribution of arsenic in natural waters. Applied Geochemistry. 2002; 17:517–568.

Sullivan KA, Aller RC. Diagenetic cycling of arsenic in Amazon shelf sediments. Geochimica et Cosmochimica Acta. 1996; 60:1465–1477.

Tokunaga TK, Wan J, Kim K, Sutton SR, Lanzirotti A, Rao W. Real-time x-ray absorption spectrscopy of uranium, iron, and manganese in contaminated sediments during bioremediation. Environmental Science & Technology. 2008; 42:2839–2844. [PubMed: 18497132]

van Geen A, Horneman A, Aziz Z, Hoque MA, Shamsudduha M, Cheng ZQ, Dhar RK, Versteeg R, Steckler M, Mailloux B, Zheng Y, Stute M, Goodbred SL, Ahmed KM. Spatial variability of arsenic concentrations and sediment properties in Bangladesh aquifers. Abstracts of Papers of the American Chemical Society. 2003; 226:U583–U583.

van Geen A, Rose J, Thoral S, Garnier JM, Zheng Y, Bottero JY. Decoupling of As and Fe release to Bangladesh groundwater under reducing conditions. Part II: Evidence from sediment incubations. Geochimica Et Cosmochimica Acta. 2004; 68:3475–3486.

Wovkulich K, Mailloux BJ, Lacko A, Keimowitz AR, Stute M, Simpson HJ, Chillrud SN. Chemical Treatments for Mobilizing Arsenic from Contaminated Aquifer Solids to Accelerate Remediation. Applied Geochemistry. 2010; 25(10):1500–1509. [PubMed: 21076621]

Zhang SZ, Li W, Shan XQ, Lu AX, Zhou PJ. Effects of low molecular weight organic anions on the release of arsenite and arsenate from a contaminated soil. Water Air and Soil Pollution. 2005; 167(1–4):111–122.

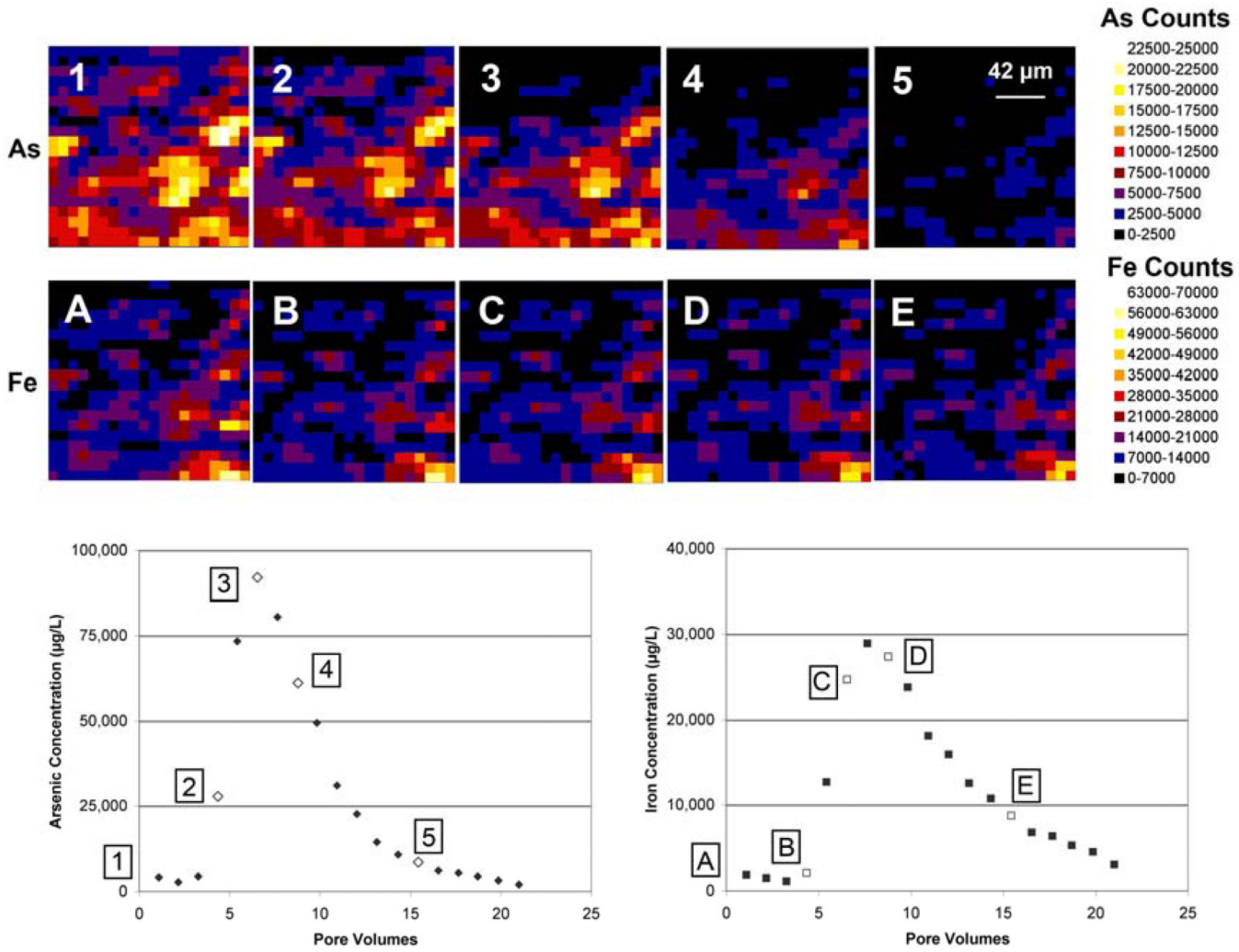

Figure 1.

µSXRF maps showing As and Fe counts in a 0.168 mm × 0.168 mm section of column #90 before (1 for As and A for Fe) and during (2–5 for As and B–E for Fe) treatment with 10 mM oxalic acid. Flow direction is from the bottom of the map to the top. For reference, maps are correlated with points on the effluent concentration vs. pore volumes graph of laboratory column #73. Arsenic map #1 and Fe map A were collected prior to introduction of oxalic acid. Arsenic maps #2–5 and Fe maps B–E were matched with the closest effluent measurement in column #73 based on number of pore volumes (open symbols).

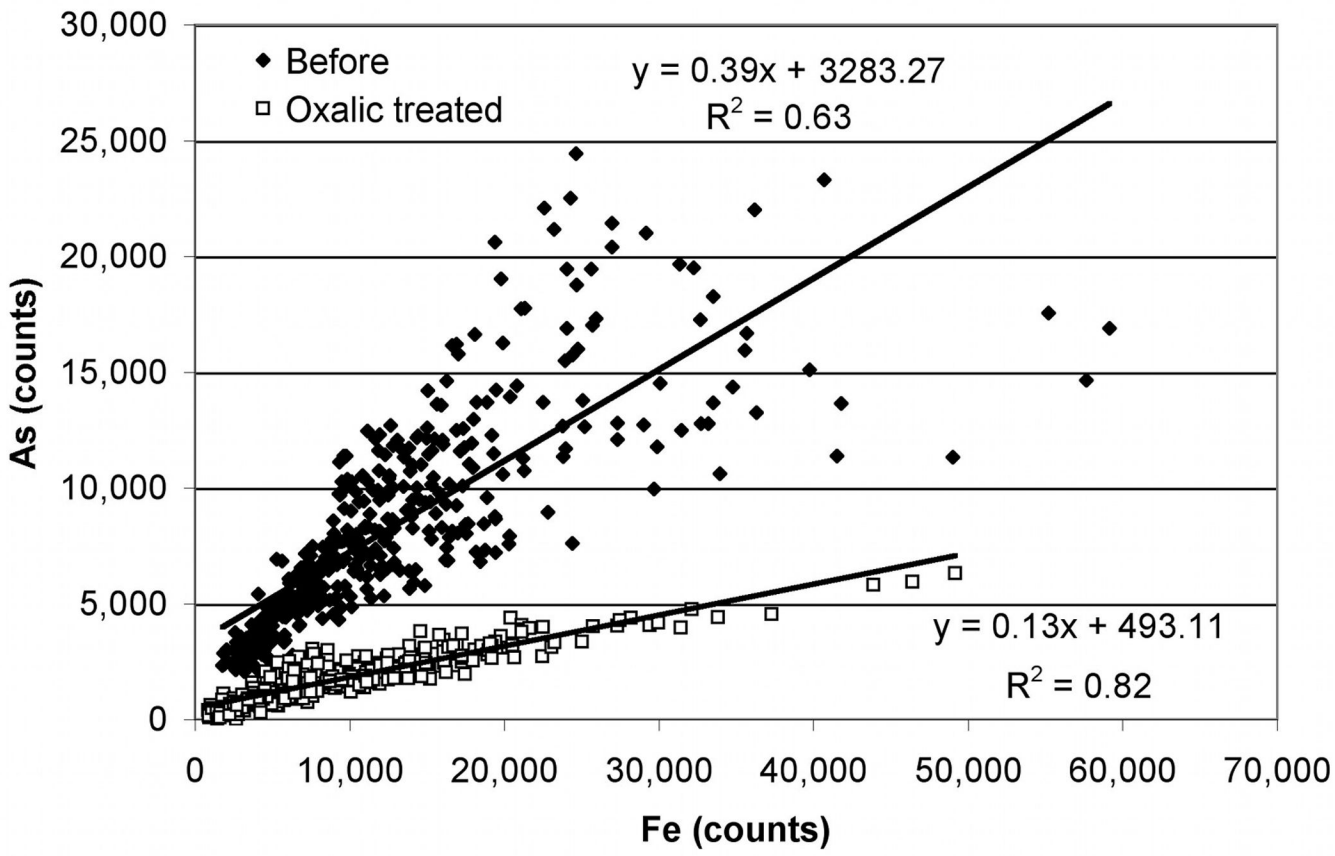

Figure 2.
Correlations between As and Fe counts from μSXRF measurements before and after oxalic acid treatment. The equation for each line and the R^2 values are shown.

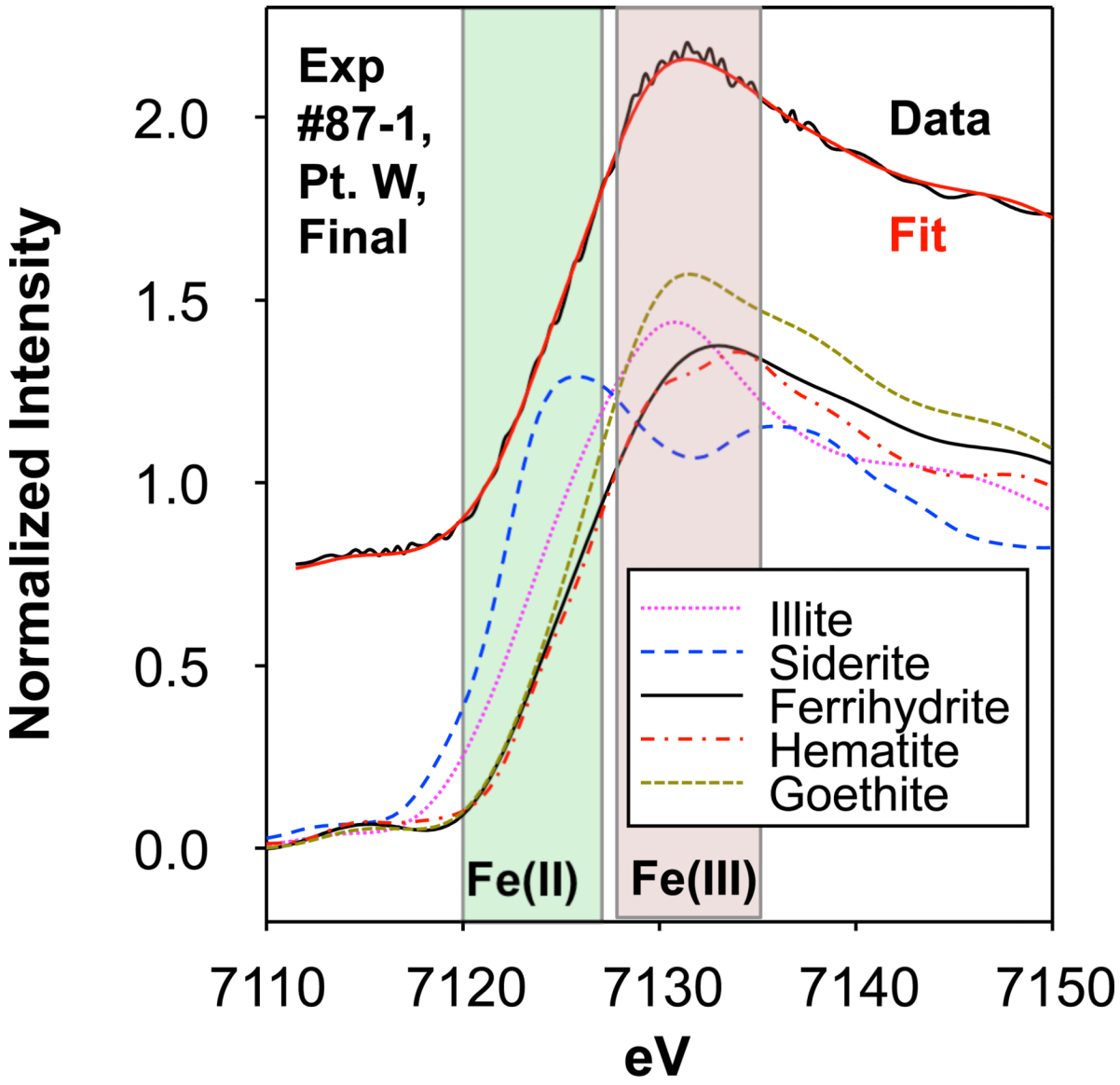

3a

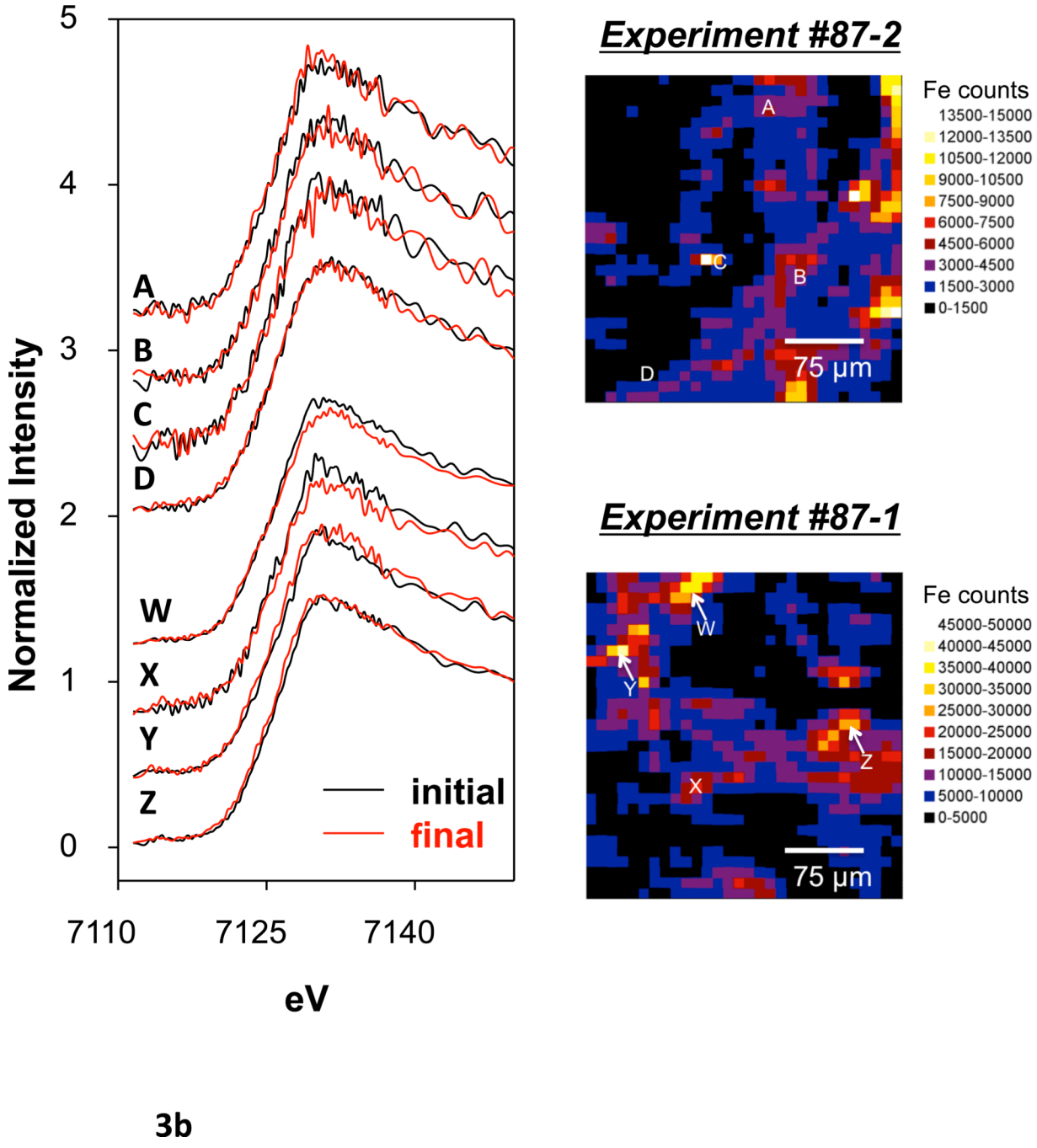

3b

Figure 3.

(a) An example μXANES fit for experiment #87-1, point W before and after oxalic acid treatment as well as Fe standards used in the fitting. (b) μXANES fits for sample points before and after oxalic acid treatment. Fe distribution maps showing the location of each sample point are included at the side.

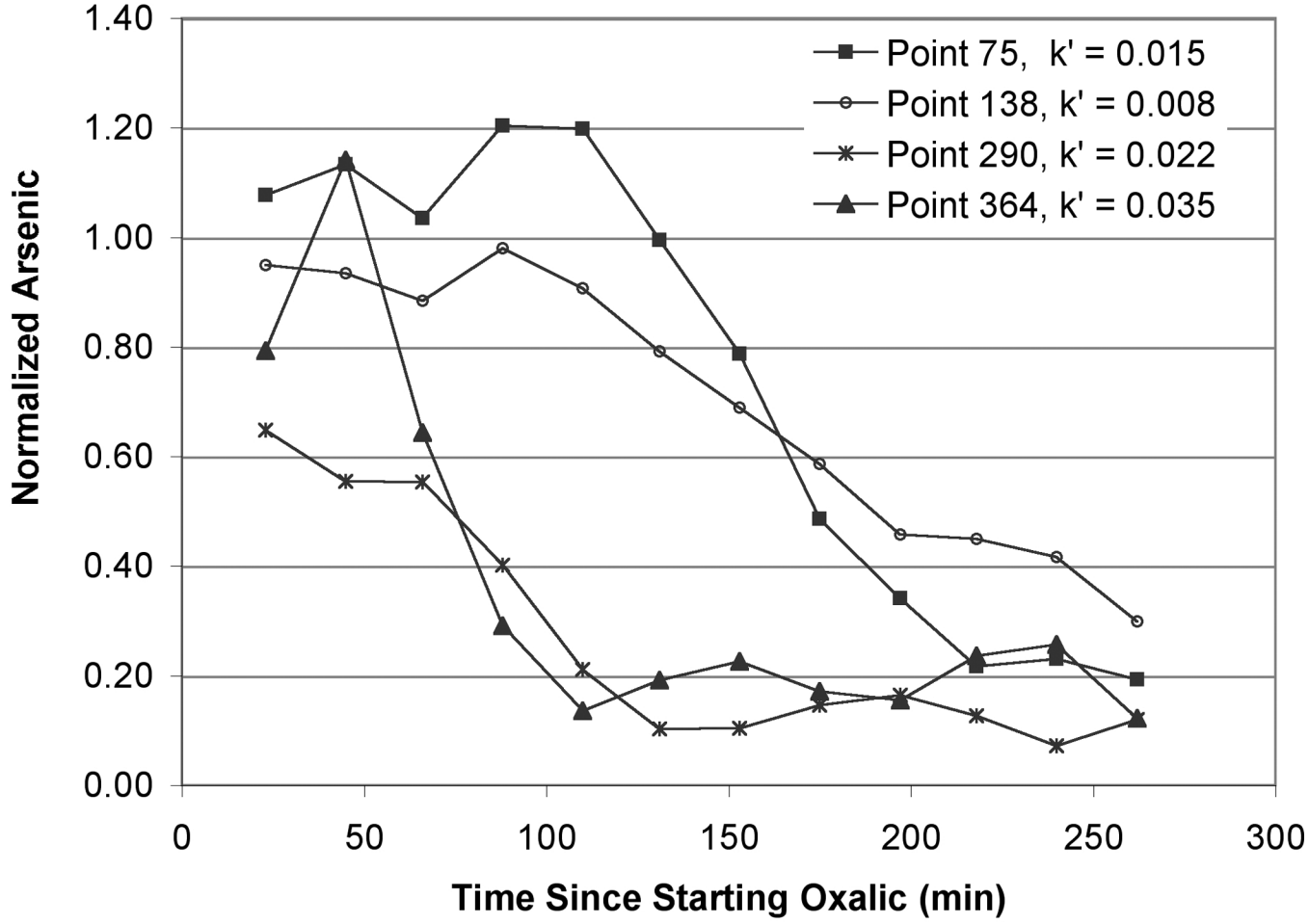

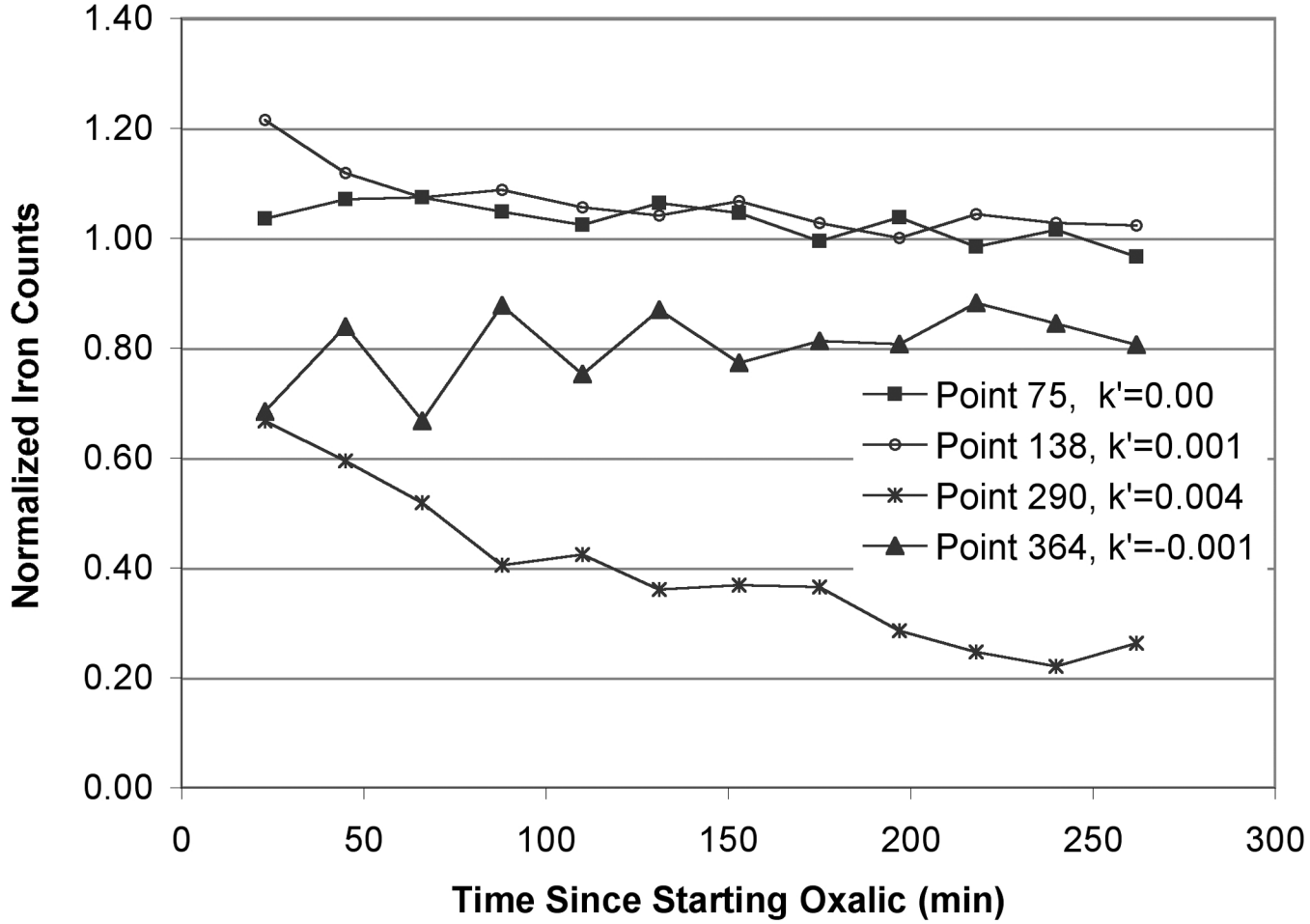

Figure 4.

(a) Normalized As counts over time as measured by μSXRF. Arsenic counts were normalized to values of the scan taken prior to oxalic acid introduction. Arsenic removal rate constants (min^{-1}) are shown for reference. The rate constants were calculated from the linear portion of graphs of Ln normalized counts vs. time.

(b) Normalized Fe counts over time as measured by μSXRF. Fe counts were normalized to values of the scan that was taken prior to oxalic acid introduction. Fe removal rate constants (min^{-1}) are shown for reference. The rate constants were calculated from the linear portion of graphs of Ln normalized counts vs. time.

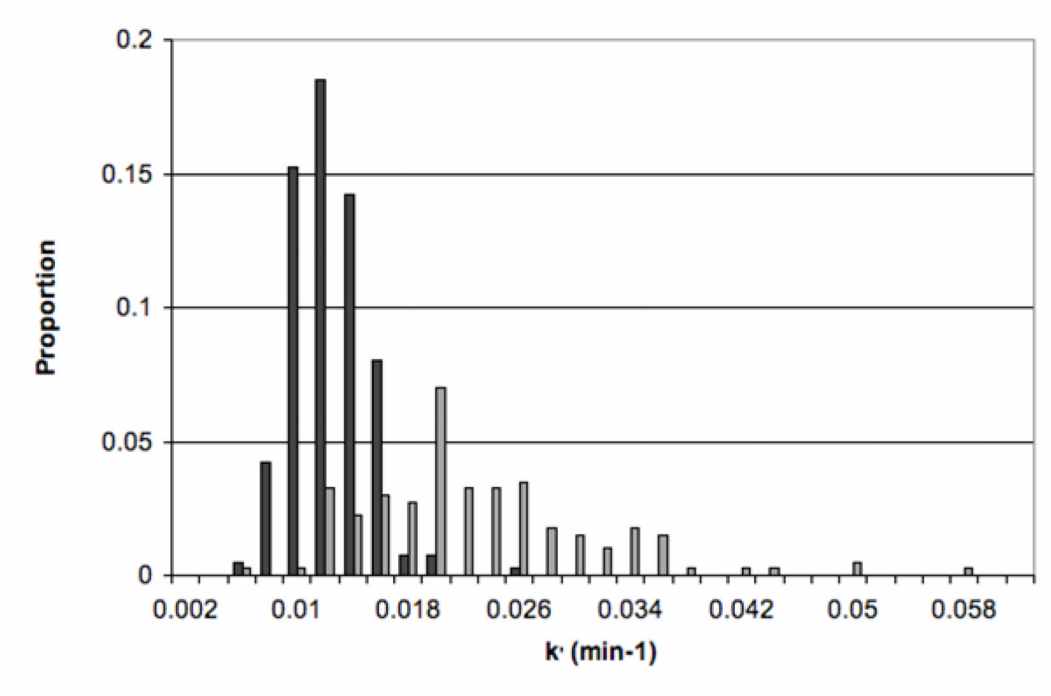

5a

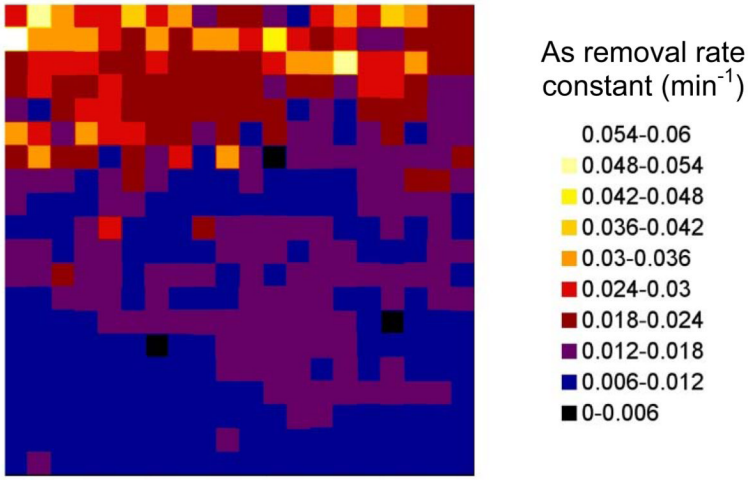

5b

Figure 5.

Distribution of rate constants for As removal. (a) Histogram showing the proportion of different rate constants of As removal in the section of column #90 analyzed by μSXRF. The darker grey bars show data for pixels #1–250 (lower portion of the analysis area) and the lighter grey for pixels #251–400. All frequency values were divided by the total number of pixels (400) to calculate the proportion. (b) Map showing the same data. Flow direction is from the bottom of the map to the top. Average standard error is 0.002 in the rate constant calculations.

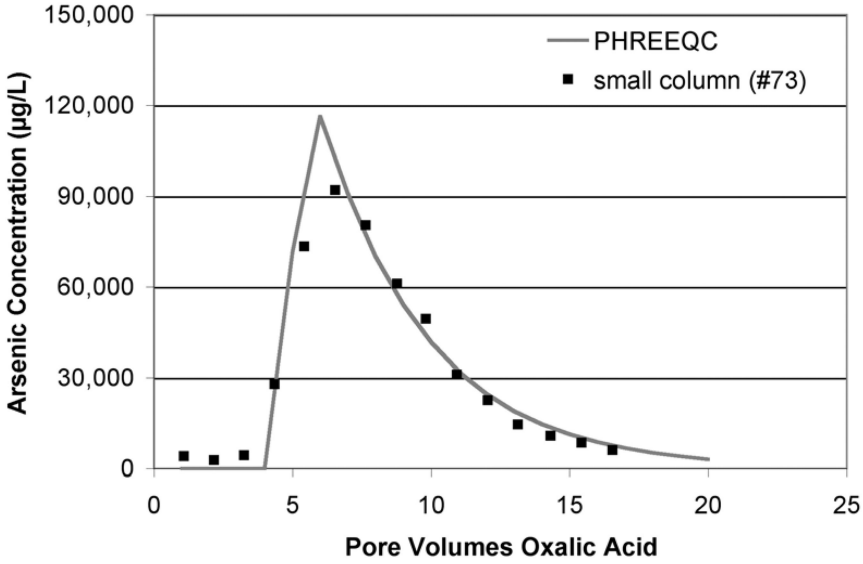

6a

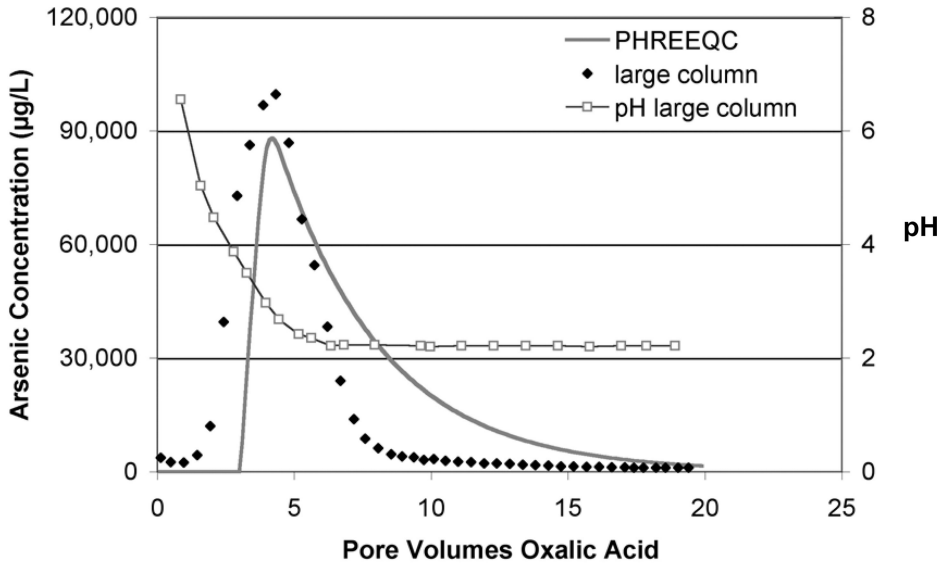

6b

Figure 6.

(a) Comparison between PHREEQC simulated effluent As concentrations and laboratory data for a small column (#73) over several pore volumes of oxalic acid treatment. A bulk average As removal rate (pv^{-1}) was calculated from the µSXRF data and used in the PHREEQC simulation; a 4 pore volume lag period was applied in the simulation. (b) Comparison between PHREEQC simulated effluent As concentrations and laboratory data for a large column (~23 cm) over several pore volumes of oxalic acid treatment. A bulk average As removal rate (pv^{-1}) was calculated from the µSXRF data and used in the PHREEQC simulation; a 3 pore volume lag period was applied in the simulation. Effluent pH values were also plotted for the large column.

Table 1

Percent As removed on the basis of μSXRF data in columns undergoing 10 mM oxalic acid treatment

	Percent As Removed Based on μSXRF Data (%)			
Experiment	**Median**	**Mean**	**Standard Deviation**	**Mode[c]**
#90[a]	80%	79%	9%	80–85%
#87-2[b]	84%	83%	8%	85–90%

[a] Each scan took approximately 20 minutes and covered an area of 0.168 mm × 0.168 mm. Total number of pixels = 400.

[b] One scan was performed before and one after oxalic acid treatment. The scans covered an area of 0.3 mm × 0.3 mm. Total number of pixels = 930.

[c] Most common value was based on histogram transformation of the data points. Data were collected into bins of 5 percentage points.

Table 2

Percent Fe removed on the basis of μSXRF data in columns undergoing 10 mM oxalic acid treatment

	Percent Fe Removed Based on μSXRF Data (%)			
Experiment	**Median**	**Mean**	**Standard deviation**	**Mode[c]**
#90[a]	30%	25%	32%	≤ 0 %[d]
#87-2[b]	15%	14%	14%	15−20%

[a] Each scan took approximately 20 minutes and covered an area of 0.168 mm × 0.168 mm. Total number of pixels = 400.

[b] One scan was performed before and one after oxalic acid treatment. The scans covered an area of 0.3 mm × 0.3 mm. Total number of pixels = 930.

[c] Most common value was based on histogram transformation of the data points. Data were collected into bins of 5 percentage points. All numbers ≤ 0 % were lumped into one bin.

[d] Percent Fe removed less than 0 indicates precipitation or re-adsorption of Fe at those pixels, rather than removal.

Table 3

Percentage of Fe species before and after oxalic acid trseatment, μXANES fits

Column #87-1					
Sample point[a]	**Percentage of Total**[b]				
	Fe-Illite	**Fh**	**Gt**	**Hm**	**Fit χ^{2}**[c]
W (before)	12±6%	13±10%	45±4%	30±4%	0.21
W (after)	14±6%	0±10%	52±4%	34±4%	0.17
X (before)	4±6%	23±10%	55±4%	18±4%	0.20
X (after)	8±6%	0±10%	71±4%	21±4%	0.23
Y (before)	3±5%	22±10%	57±4%	18±4%	0.11
Y (after)	6±5%	0±10%	65±4%	29±4%	0.17
Z (before)	2±5%	21±10%	66±4%	11±4%	0.20
Z (after)	2±5%	0±10%	73±4%	25±4%	0.16
Column #87-2					
Sample point	**Percentage of Total**[b]				
	Fe-Illite	**Fh**	**Gt**	**Hm**	**Fit χ^{2}**[c]
A (before)	12±6%	13±10%	45±4%	30±4%	0.12
A (after)	14±6%	0±10%	52±4%	34±4%	0.12
B (before)	4±6%	23±10%	55±4%	18±4%	0.13
B (after)	8±6%	0±10%	71±4%	21±4%	0.15
C (before)	3±5%	22±10%	57±4%	18±4%	0.10
C (after)	6±5%	0±10%	65±4%	29±4%	0.09
D (before)	2±5%	21±10%	66±4%	11±4%	0.16
D (after)	2±5%	0±10%	73±4%	25±4%	0.17

[a] Sample points D and Z had elevated As counts in the before treatment map; sample points C, X, and Y had elevated Fe counts in the before treatment map; sample points A, B, and W had elevated counts in both elements in the before treatment map.

[b] Fe-illite is Fe(III)-rich illite, Fh = Ferrihydrite, Gt = goethite, Hm = hematite. Siderite was used as the representative Fe(II) mineral; it and others, including, sulfides were not significant and are not included in final fits. Fits were normalized to 100%. Errors are calculated from fitting in Six Pack.

[c] The χ^{2} is a statistical parameter related to goodness of fit.

Table 4

Parameters for PHREEQC Models

Relative Column Size	**Small (#73)**[a]	**Large**[b]
Sediment Properties		
As concentration (mg/kg)	86	81
Porosity	0.27	0.33
Column Properties		
Total column length (cm)	4.25	23.5
Time/pore volume (min)	18	158
Other PHREEQC inputs		
# Cells	20	20
# Shifts	400	400
Length/cell (cm)	0.2125	1.175
Time step (s)	54	475
Total # pore volumes	20	20
# Pore volumes lag	4	3
As removal rate (pv^{-1})	0.2608	0.2608

[a] Small column parameters are based on lab bench column #73, except for As removal rate which was derived from synchrotron column #90.

[b] Large column parameters are based on a 23.5 cm long lab bench column (Wovkulich et al., 2010), except for As removal rate which was derived from synchrotron column #90.